



**COMPARATIVE MEASUREMENTS OF THE UNSTEADY PRESSURES
AND THE TIP-VORTEX PARAMETERS ON FOUR
OSCILLATING WING TIP MODELS**

BY

WOLFGANG J. WAGNER

German Aerospace Research Establishment (DFVLR)

Institute of Aeroelasticity

Göttingen, W. Germany

TENTH EUROPEAN ROTORCRAFT FORUM

AUGUST 28 – 31, 1984 – THE HAGUE, THE NETHERLANDS

Comparative Measurements of the Unsteady Pressures and the Tip-Vortex
Parameters on Four Oscillating Wing Tip Models

by

Wolfgang J. Wagner

Abstract

Experimental investigations on steady and unsteady pressure distributions and on the tip vortex qualities of four wing tip configurations (rectangular tip, Ogee tip, trapezoidal tip, swept tip) are presented and discussed. The tip vortex qualities were investigated by means of an ultrasonic measuring device. The results give insight into the finer structure of the vortices and supply information on vortex position, core diameter and maximum velocity as well as vortex behaviour if the blade is oscillated. This is demonstrated by a selection of a few single conditions.

Notation

| | |
|----------------|--|
| α | angle of attack |
| $\Delta\alpha$ | amplitude of oscillation |
| c_p | pressure coefficient |
| c_p' | real part of dynamic pressure coefficient |
| c_p'' | imaginary part of dynamic pressure coefficient |
| f | frequency of blade oscillation |
| r | radius relative to the center of the vortex |
| r_0 | radius of vortex core |
| Δt_w | flow-induced differences of ultrasonic pulse running times |
| $v = u_\infty$ | free-stream velocity |
| x/ℓ | chordwise coordinate |

1. Introduction

In order to improve helicopters there are numerous good arguments dealing with the rotor blades and especially with their tips. A score of undesirable effects seem to originate there, such as excessive noise, vibration which affects the entire structure, loss of energy and negative influence on structures in the wake of the blade tips.

The following contribution shows the influence of shape variation of the blade tip configurations on the tip vortex and on the pressure distributions on the surface. For this purpose four discrete shapes have been chosen:

1. Rectangular,
2. Ogee,
3. Swept and
4. Trapezoidal.

A NACA 0012 profile and other geometrical parameters are chosen as equal for all configurations as possible.

A parallel contribution to this Rotorcraft Forum by W. Send entitled "Theoretical Prediction of Running-Time Measurements in Unsteady Flows" uses the same ultrasonic measuring data for comparison with his calculations.

Figure 1: The four wing models tested. ▶

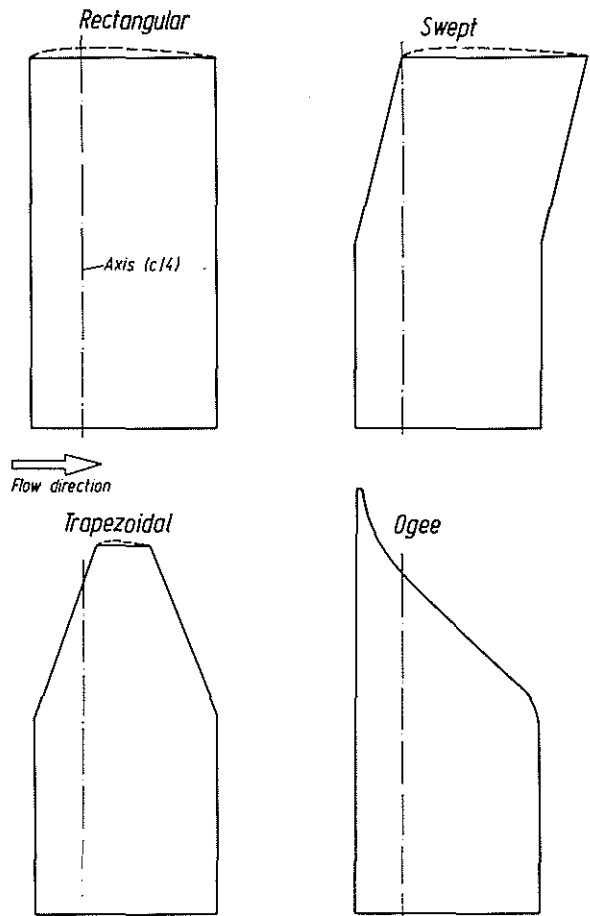
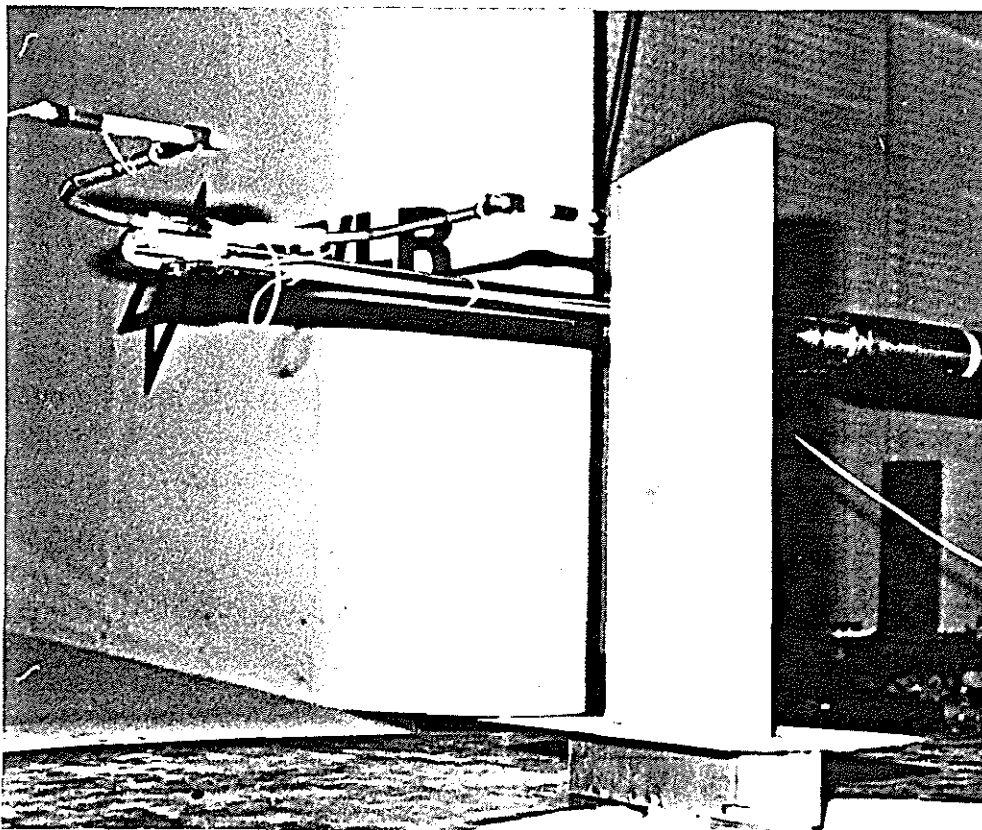


Figure 2: Photo of the rectangular wing model and the ultrasonic microphone setup in wind-tunnel. ▼



2. Experimental setup

A sketch of the four wing models tested appears in Figure 1. The test models used here have NACA 0012 profiles of chordlength $c = 400$ mm at the base. All models have the same basic shape up to a span of $s = 400$ mm.

The experimental setup must fulfill two purposes: first, to provide an opportunity to measure steady and unsteady pressures and second, to allow the tip vortex parameters of interest to be measured with an ultrasonic device. A photo (Figure 2) of the rectangular wing model demonstrates the typical setup in the windtunnel. In the left corner of the photo the ultrasonic microphone system which is mounted on a traversing mechanism can be seen. All parts of the setup having to do with the supports, the hydraulic shaker and signal lead cables are protected from the airflow by a floor plate.

Figure 3 is a block diagram of the entire test setup for measuring steady and unsteady pressures, including the hydraulic, electronic and data-processing components. The time-tryed method of pressure measurements using a tube/pressure-measuring selector/precision pressure-sensor system was employed [6]. The measuring equipment was supplemented for the present investigations by a PDP 11/34 computer. Thus it was possible to control 7 scanivalve pressure-measuring selectors simultaneously with an interface and to store the test data obtained.

The second part of the test setup is the ultrasonic measuring device. According to Figure 4 a short ultrasonic pulse is transmitted by a sender microphone. After having crossed a fixed distance (ca. 50 cm) the ultrasonic pulse is picked up by a receiving microphone. If the flow has a velocity component in the direction of the path of the sound wave, the running time of the ultrasonic pulse is altered.

$$\Delta t = \int_{\ell} \frac{dz}{c - w(x,y,z)} - \int_{\ell} \frac{dz}{c}, \quad (1)$$

where c is the velocity of sound and $w(x,y,z)$ is the velocity field of the flow.

The microphone system is mounted on a traversing mechanism, allowing it to be shifted to every point in the test section. In doing so, one wins a distribution of running times with respect to location. If there is a vortex (or two vortices) in the test section one can assume a theoretical model for its velocity field. We have used a Hamel-Oseen vortex model in this investigation, which is a vortex representing a flow field in which the velocity starts with $u = 0$ at $r = 0$, reaches a maximum at r_0 (the vortex core radius) and, at large values of r , follows the law valid for a potential vortex with u approaching zero asymptotically. The following formula expresses this behaviour.

$$\frac{u}{u_{\max}} = 1.4 \frac{r_0}{r} \left[1 - \exp\left(\frac{-1.26 r^2}{r_0^2}\right) \right]. \quad (2)$$

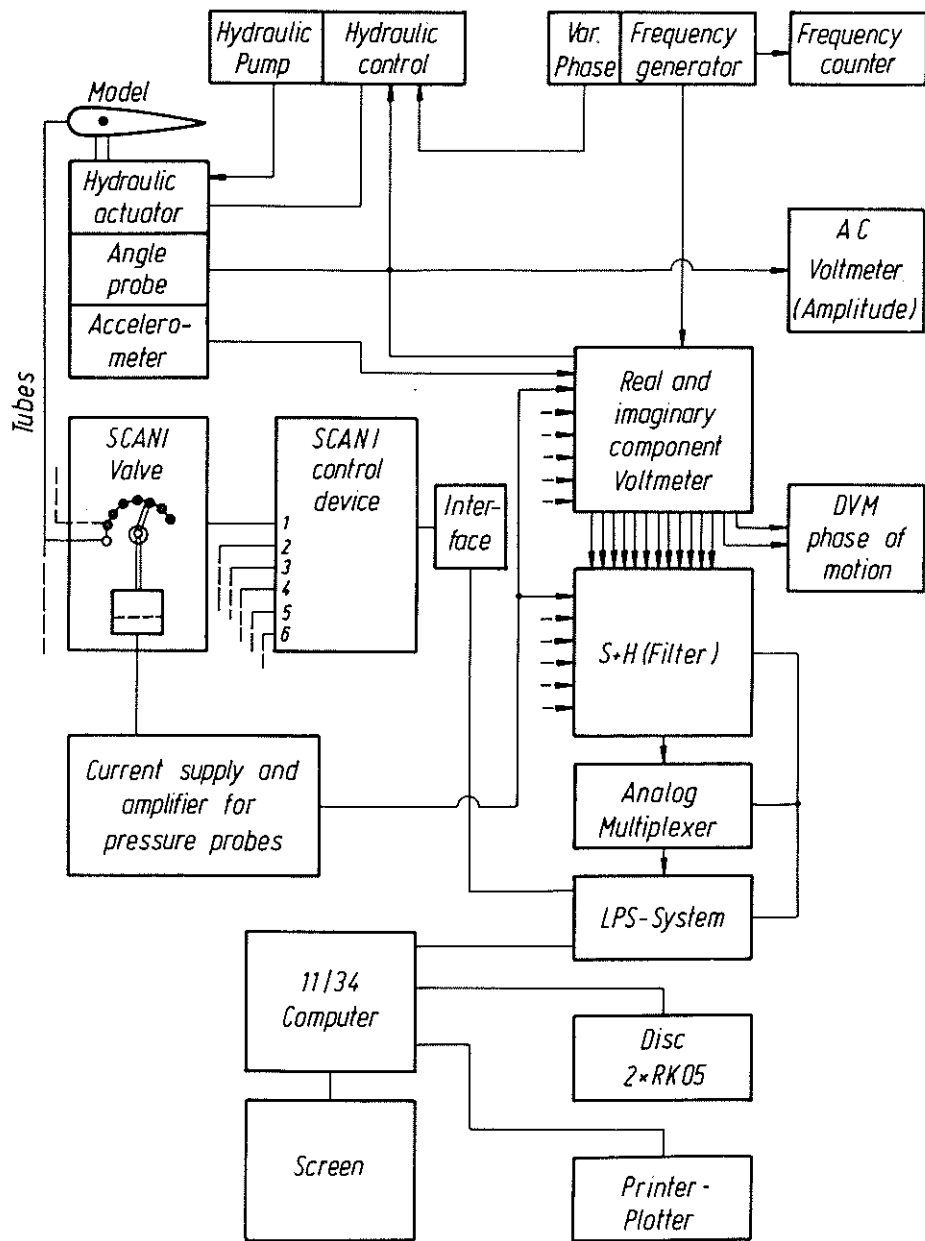


Figure 3: Block diagram of test setup for measuring unsteady pressures.

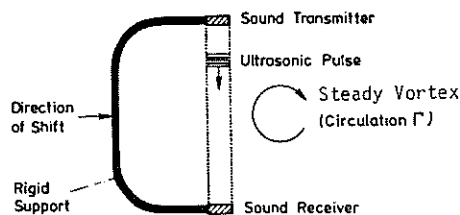


Figure 4: Schematic view of a single ultrasonic test beam.

The blade tip models are also induced to perform sinusoidal oscillations about their quarter-chord axis by means of a hydraulic shaker. In order to measure the tip vortices of the oscillating blade it was necessary to acquire data (running times) quickly and to synchronise them with the mechanical motion. The maximum required rate was 440 single running-time values per second. The schematic diagram of the electronic and data-acquisition setup is shown in Figure 5. In a simplified way one can describe the procedure as follows: each period of the blade oscillation is divided into 32 intervals of equal length. One complete measurement of the running time is performed in each of these 32 intervals and the data are stored in the computer memory. By shifting the microphone setup through the measuring section, the behaviour of the vortex during one period of blade oscillation can be observed with a resolution of 32 pictures.

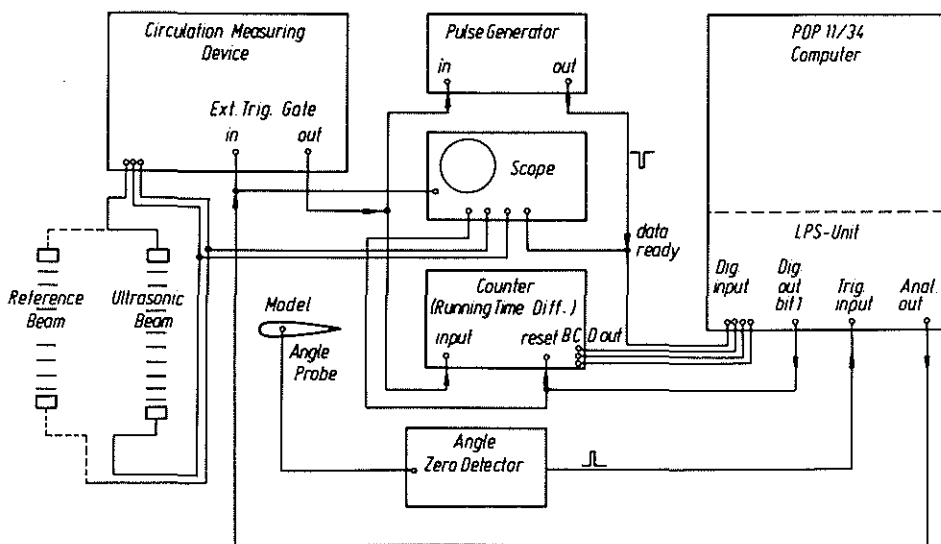


Figure 5: Schematic diagram of ultrasonic test setup for acquisition and processing of data.

Figure 6: Variation of running time with position, $U_\infty = 20$ m/s, $x/l = 5$, $\alpha_0 = 5^\circ$. Calculated core based on one Hamel-Oseen vortex.

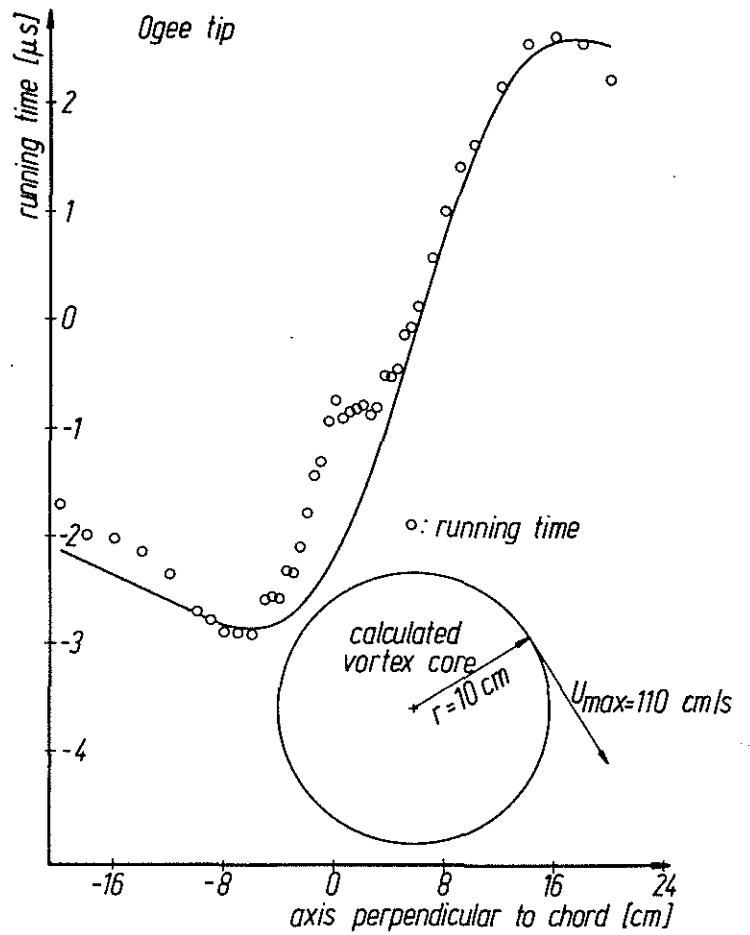
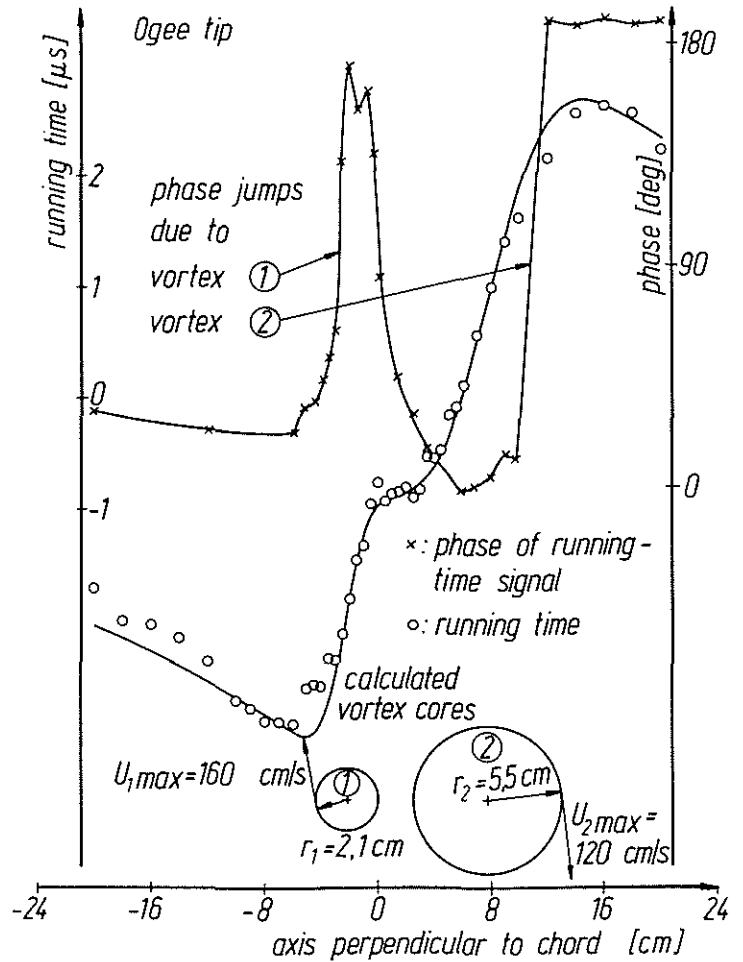


Figure 7: Variation of running time and phase of running time (model with forced pitching oscillations) with position, $U_\infty = 20$ m/s, $x/l = 5$, $\alpha_0 = 5^\circ$, $\Delta\alpha = \pm 1^\circ$, $f = 4$ Hz. Calculated core based on two Hamel-Oseen vortices.



In order to illustrate the kind of problems and results which thus arise, Figures 6 and 7 demonstrate the running-time measurements at a fixed time interval in the wake of the Ogee tip. In both figures the same measuring points are drawn. In Fig.6 the solid line is the calculated best-fit curve based on one Hamel-Oseen vortex. As a result, one can see a large vortex core with a radius of 10 cm and a maximum velocity of $u_{\max} = 120$ cm/s. This would be a good result for the intention of reducing the vortex velocity, but the curve fit is not very convincing. In Fig.7 the calculated best-fit curve is based on two Hamel-Oseen vortices which are superimposed. The curve fit is now much better than in Fig.6, but does this make sense with respect to physics? Fortunately we have additional time-dependent information because of the 32 measurements taken during one oscillation period of the model. Based on this time signal we have calculated the phase with respect to the model motion. The upper solid curve represents this phase. Coming from the left side, this curve shows two jumps of 180 deg with a transition region between them. These jumps correspond quite exactly with the middle position of the two calculated vortex cores. It is easy to see that the phase of the running-time signal is indeed shifted by 180 deg as the microphones pass one vortex center. The same assumption is correct for two vortices with the same sense of rotation. The refined analysis shows that the tip vortex structure of the Ogee tip consists of two vortex cores with the same sense of rotation. The maximum velocity in the vortex structure is now 160 cm/s instead of 110 cm/s in the case above.

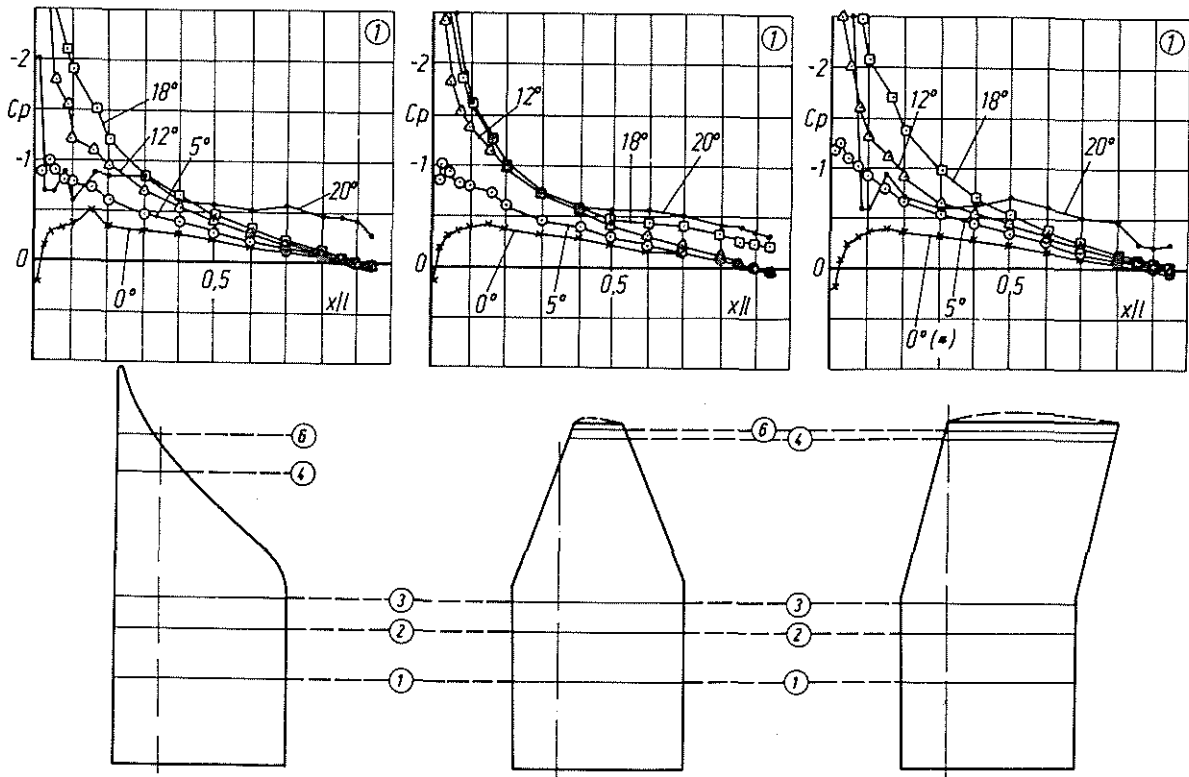


Figure 8: Changes of steady pressure on upper surface with incidence, $V = 50$ m/s.

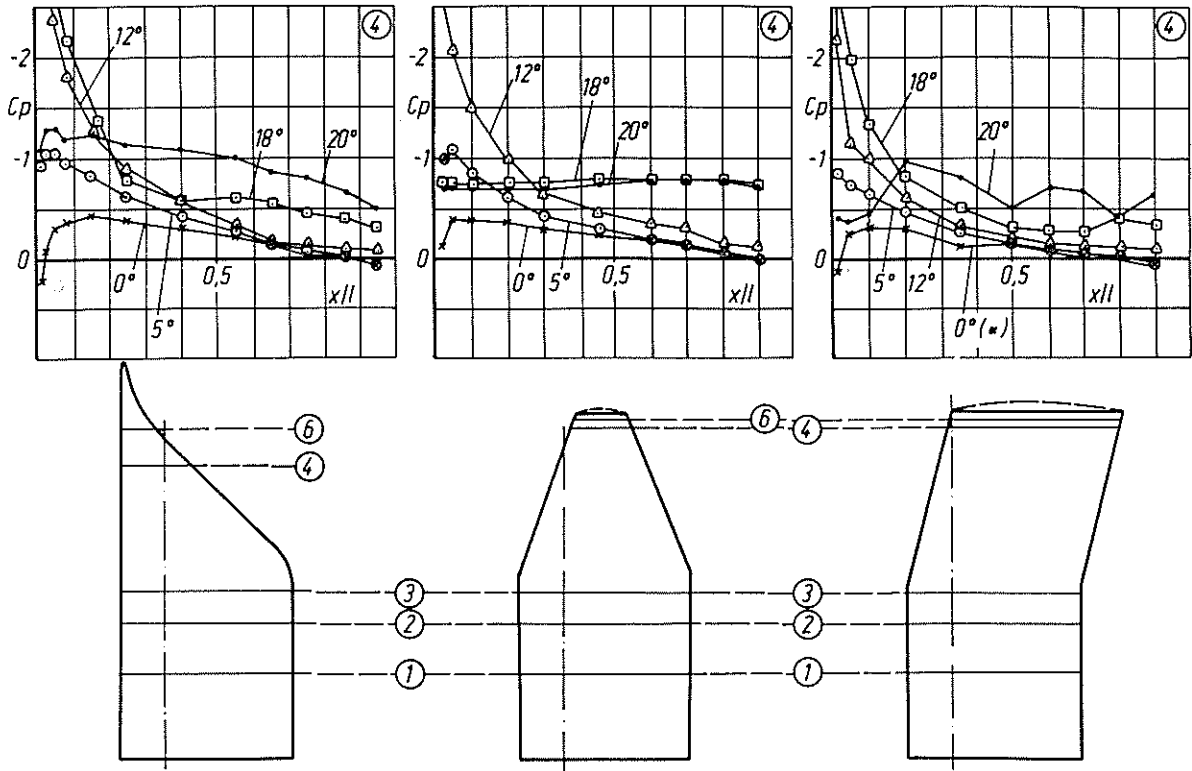


Figure 9: Changes of steady pressure on upper surface with incidence, $V = 50$ m/s.

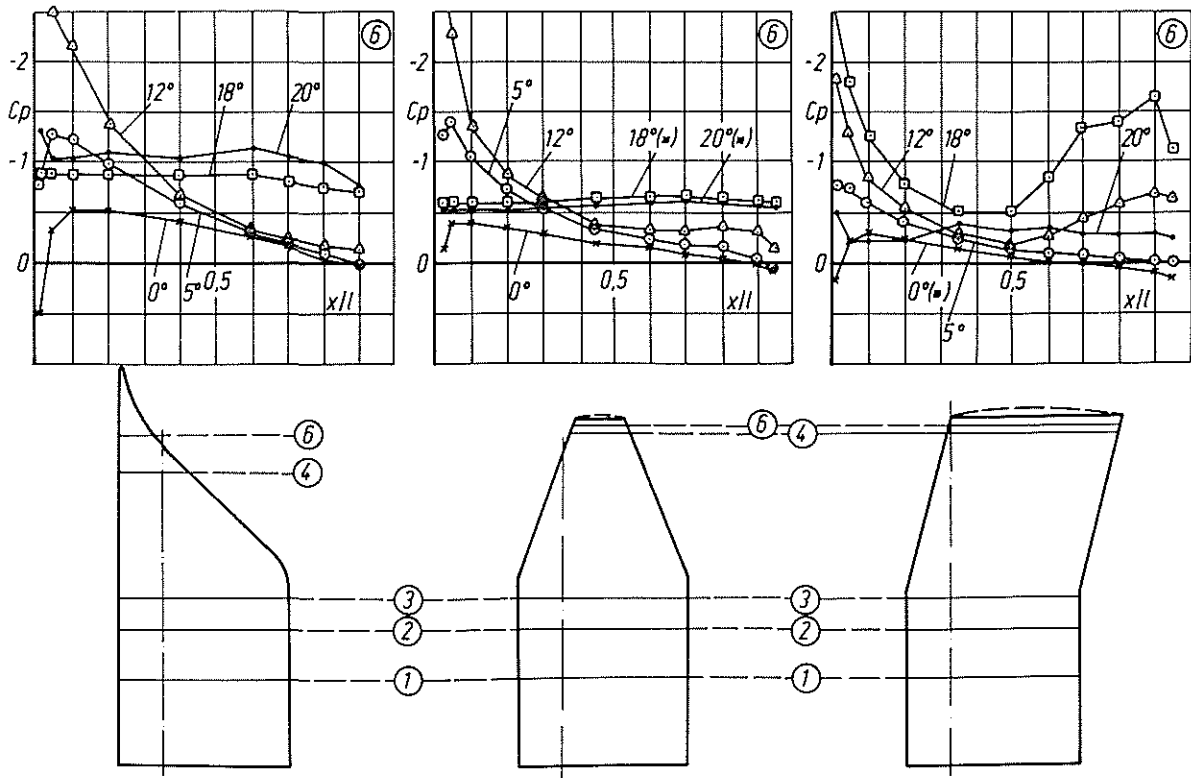


Figure 10: Changes of steady pressure on upper surface with incidence, $V = 50$ m/s.

3. Steady and unsteady pressures on the blade tips

Figures 8-10 show the changes of steady pressure on the upper surface of the three configurations tested. The measured pressures are shown as curves for 5 discrete angles of attack from 0° to 20° at three control sections. The locations of the control sections are indicated by circled numbers in the upper right-hand corners. The corresponding position on the wings is shown in the drawing underneath.

A comparison of the curves for 0° angle of attack at control section (1), Figure 8 (zone of 2-dimensional flow), shows that the curves of all three wing configurations are qualitatively similar. A quantitative deviation shows the Ogee configuration at $x/l \approx 0.15$ with a 15% higher extreme value. For 18° angle of attack the trapezoidal wing shows flow separation while the other two wings show flow separation not before 20° angle of attack beginning at the middle of the chords.

Figure 10 shows the conditions at the outer tip regions. Beginning with $x/l \approx 0.5$ the c_p -curves do not reach positive values but remain negative at the trailing edge. Here the influence of the developing tip vortices is seen in the suction zone on the blade surface below, which deepens with increasing angle of attack. An exact determination of the vortex position based on these curves is not possible, whereas this has been done with the ultrasonic method.

Figures 11 and 12 show the real and imaginary parts of unsteady pressures at the zone of 2-dimensional flow. There is nothing extraordinary to see; the curves behave as expected. The curves for 19° and 12° make no sense due to flow separation.

Figures 13 and 14 show the real parts of the unsteady pressures in the outer tip regions. One can recognise the tendency that the c_p' -values approaching the outer tip region increase at the trailing edge. This effect is strengthened by increasing angle of attack with the exception of the trapezoidal tip section (6) $\alpha = 12^\circ$. This effect is due to the tip vortices which originate there and change the vortex circulation (as well as their position, as we shall see later) with the angle of attack.

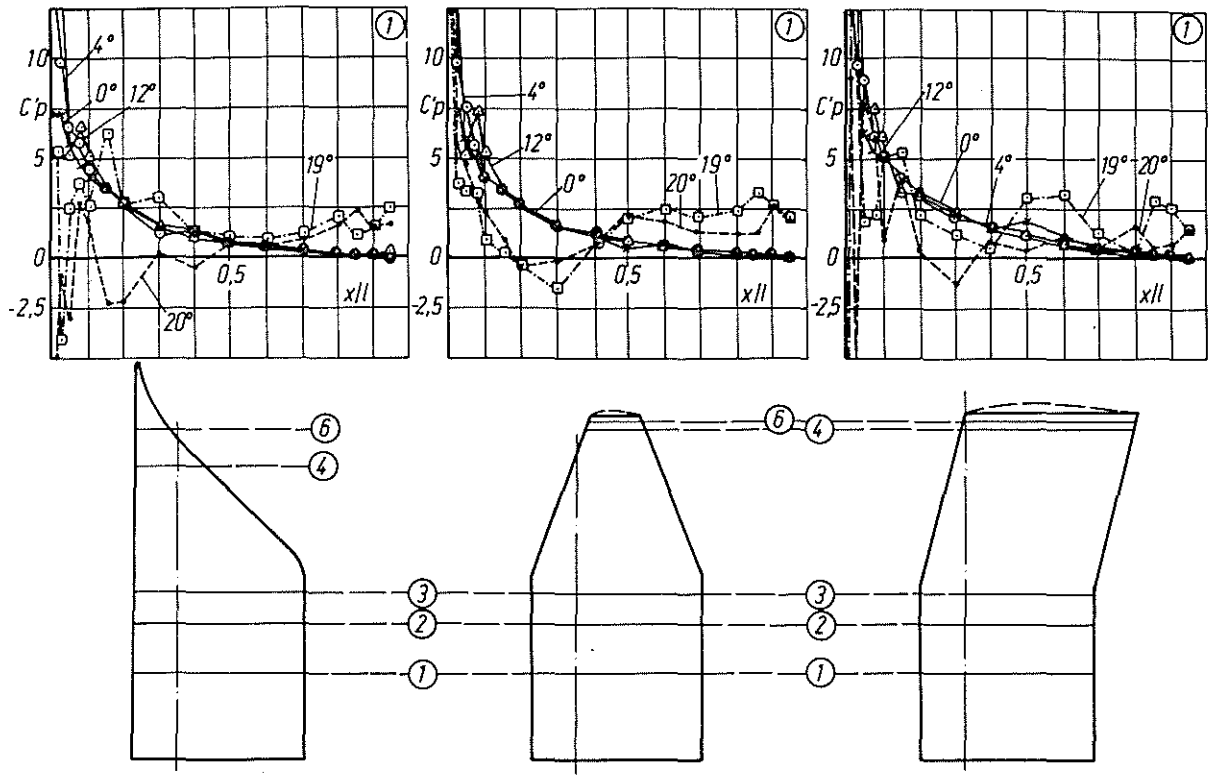


Figure 11: Unsteady pressures - real part. Effects of increasing incidence, $V = 50$ m/s, $\Delta\alpha = \pm 1^\circ$, $f = 4$ Hz.

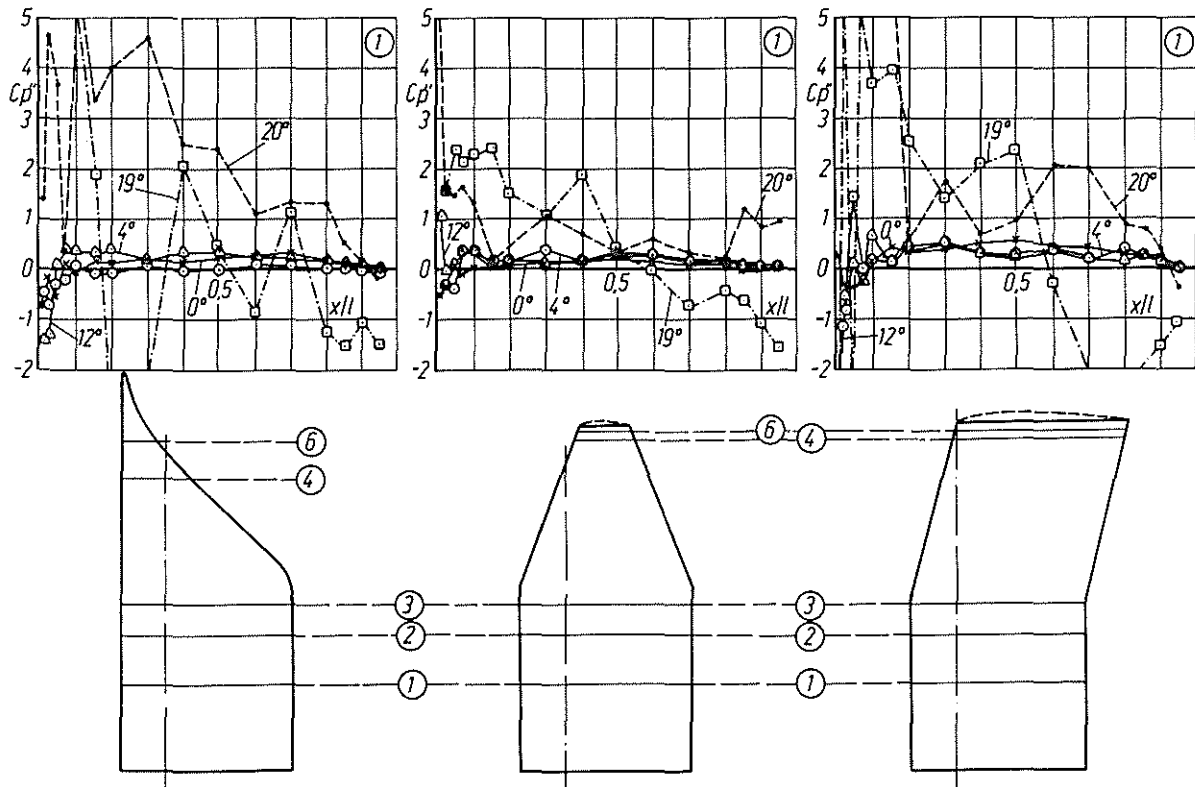


Figure 12: Unsteady pressures - imag. part. Effects of increasing incidence, $V = 50$ m/s, $\Delta\alpha = \pm 1^\circ$, $f = 4$ Hz.

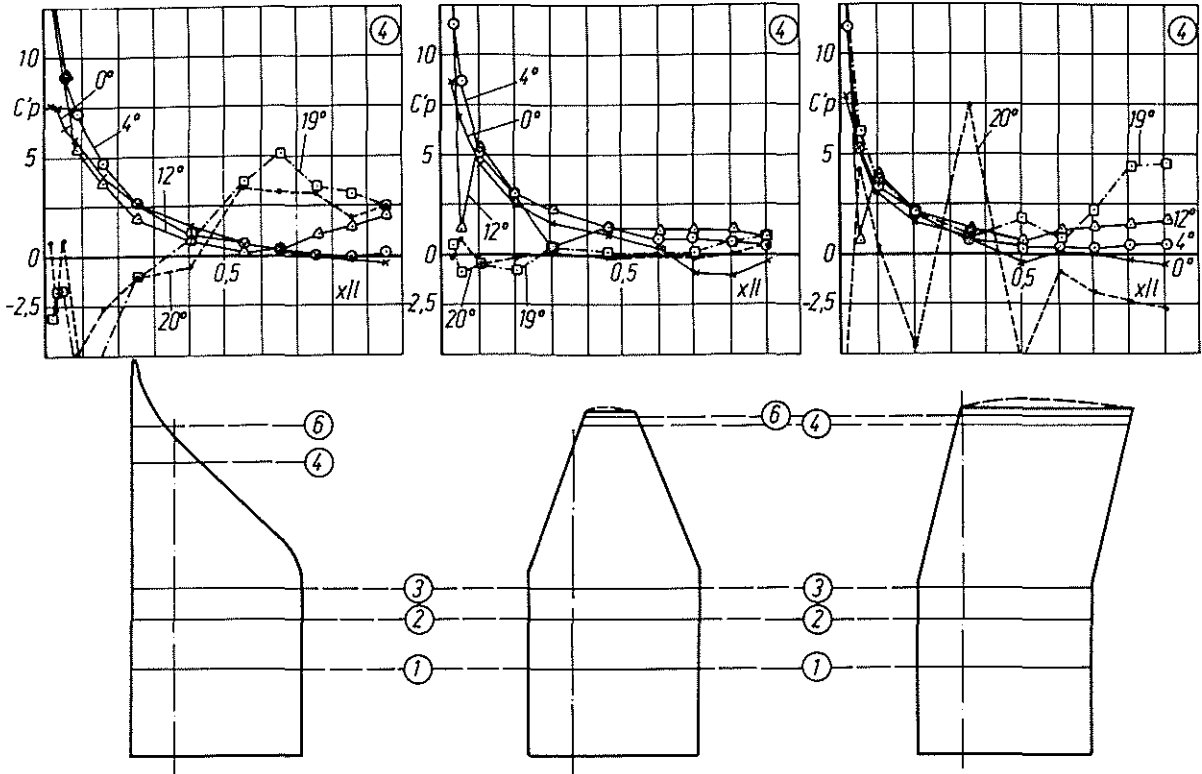


Figure 13: Unsteady pressures - real part. Effects of increasing incidence, $V = 50 \text{ m/s}$, $\Delta\alpha = \pm 1^\circ$, $f = 4 \text{ Hz}$.

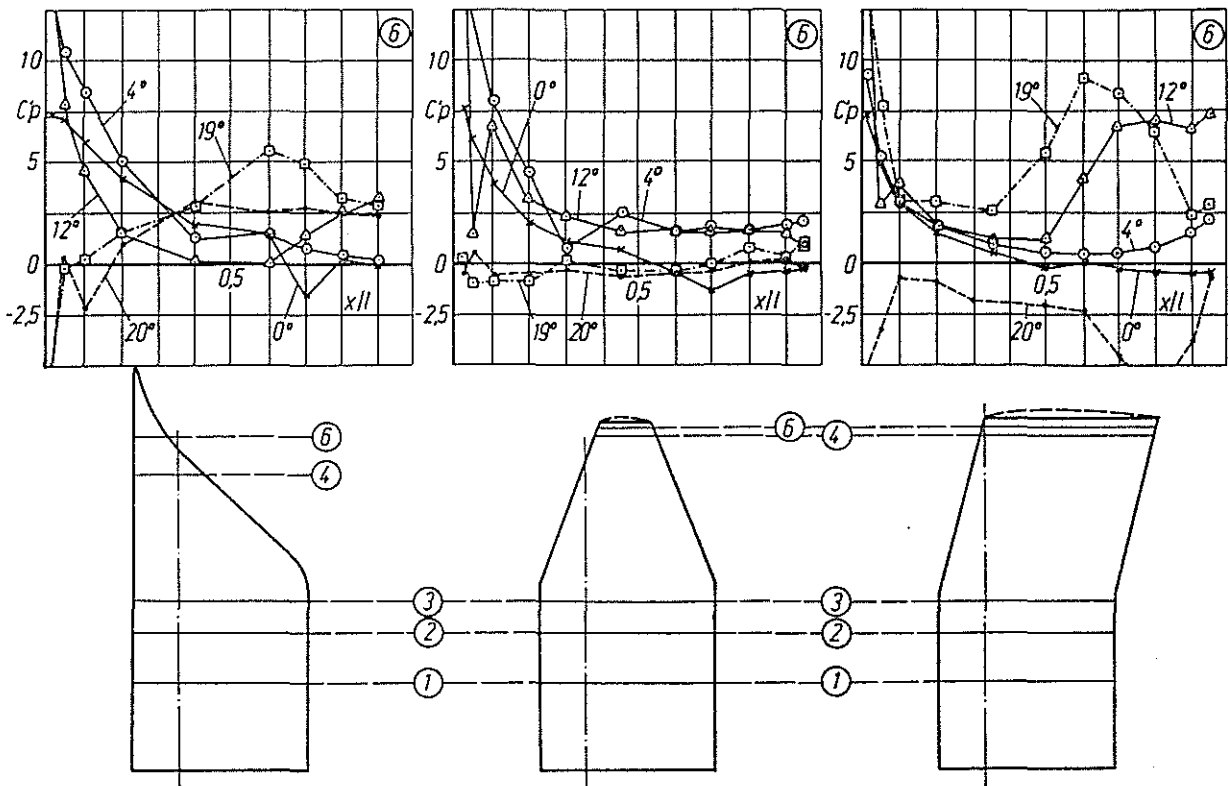


Figure 14: Unsteady pressures - real part. Effects of increasing incidence, $V = 50 \text{ m/s}$, $\Delta\alpha = \pm 1^\circ$, $f = 4 \text{ Hz}$.

4. Results concerning the tip vortices

Figures 15-18 show in a common graph the lines of equal static pressure on the upper surface of the blade tip, the ultrasonic running-time curves and the calculated vortex cores, respectively. The spanwise coordinate serves as true reference for the entire drawing. For each of the four configurations the blade tip is oscillating with a mean angle of attack of 5° and an amplitude of $\pm 1^\circ$. The two running-time curves are taken for the moment of the smallest angle of attack 4° and the moment of the largest angle of attack 6° and show therefore the extremal positions 1 and 2. The vortex core is also drawn for both extremal positions 1 and 2 if they are different.

In Fig.15 the Ogee tip configuration shows a vortex core which is oscillating between locations 1 and 2. The core diameter for the smaller angle of attack is smaller than at the larger angle. At the spanwise position of the vortex the lines of equal pressure show a concave curvature. This means that the vortex induces underpressure on the region of the surface where it originates. Because of vortex motion this region is smoother over a longer distance.

In Fig.16 the rectangular configuration shows one small vortex core which stays in a stable position independent of oscillation. The circle indicated by dashed lines shows a second vortex core in the tip vortex structure. This second core is more easily seen if one performs a measurement perpendicular to the spanwise direction, because the core is located under the plane of the main vortex which covers it partly in this graph.

In Fig.17 the trapezoidal tip configuration shows one vortex which is also oscillating in spanwise direction as does the vortex of the Ogee tip. The amplitude of oscillation is smaller than for the Ogee tip.

Fig.18 shows the swept wing configuration. The two running-time curves show no shift, which means that the vortex has a stable spanwise position independent of wing oscillation. The core radius is relatively small. The lines of equal pressure show considerable curvature: this is because the flow must accelerate and decelerate in order to follow the complicated shape of the model. The tip vortex appears on the outer tip in the form of a concave curvature of the lines indicating an underpressure field.

In order to gain insight into the time-dependent behaviour, Figures 19 and 20 show the time history of the maximum circumferential velocity and the circulation of the two tip vortices in the wake of the Ogee tip. The maximum circumferential velocity performs only small oscillations of a complicated nature, whereas the circulation fluctuates nearly sinusoidally as one would expect. We know already that the whole structure changes its position in spanwise direction. From this information one can derive that the entire vortex structure changes its inner conditions during the oscillation of the blade.

Figure 21 shows the time history of the maximum circumferential velocities of the two vortices in the tip vortex structure of the rectangular tip. In this case the change with phase is approximately sinusoidal. With this additional information it is evident that the flow over the rectangular tip is smoother than that over the Ogee tip.

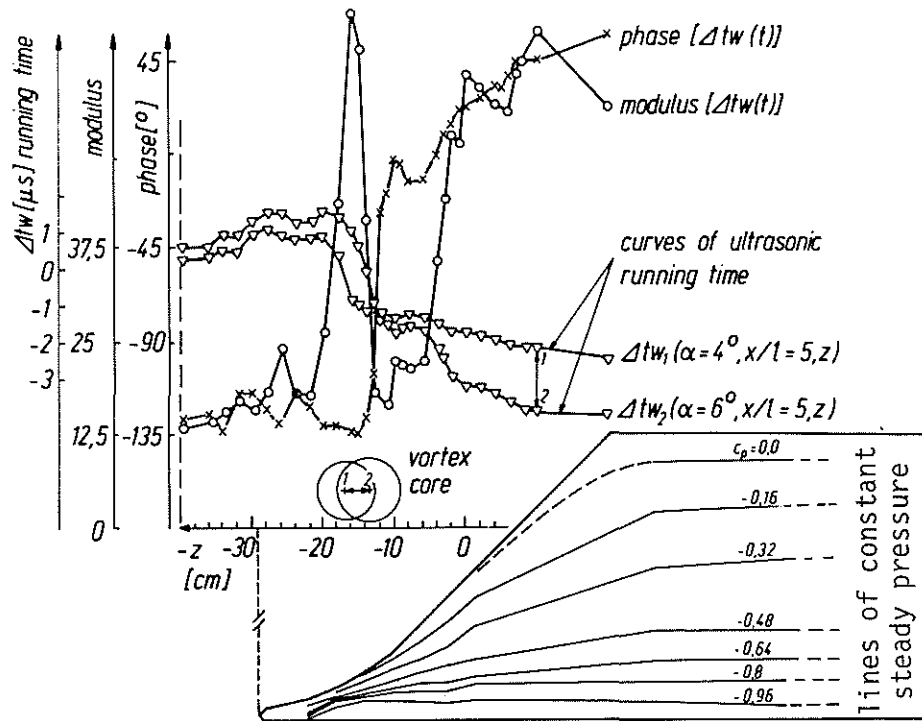


Figure 15: Graphs with equal scale in spanwise coordinate:

- ultrasonic running-time curves and curves of modulus and phase of the running-time signal
- lines of constant pressure on the upper surface of the blade tip.
- calculated vortex core (true radius and incidence-dependent z-position) $V = 20$ m/s, $\alpha_0 = 5^\circ$, $\Delta\alpha = \pm 1^\circ$, $f = 4$ Hz.

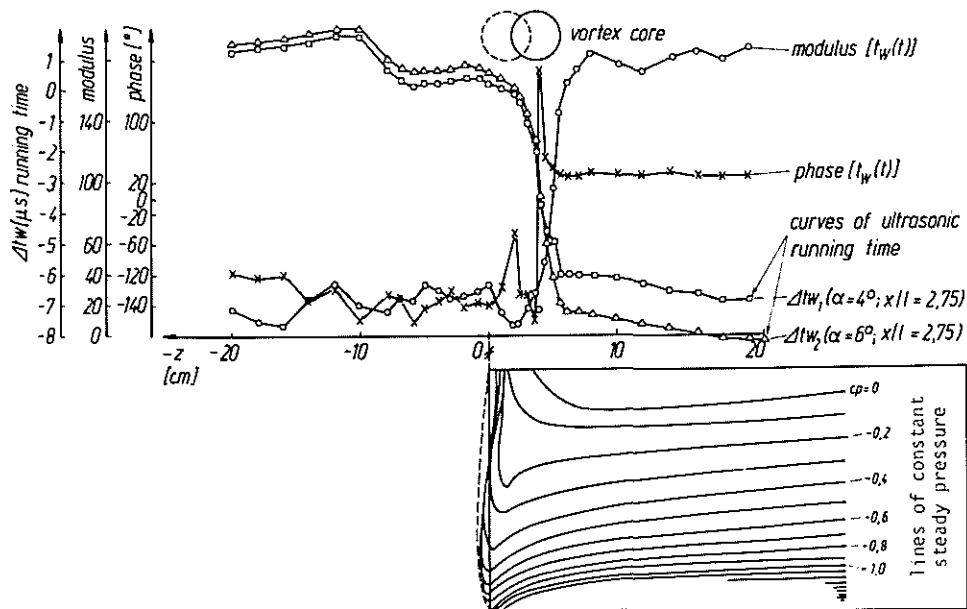


Figure 16: Graphs with equal scale in spanwise coordinate:

- ultrasonic running-time curves and curves of modulus and phase of running time signal
- lines of constant pressure on the upper surface of the blade tip.
- calculated vortex core (true radius and z-position) $V = 20$ m/s, $\alpha_0 = 5^\circ$, $\Delta\alpha = \pm 1^\circ$, $f = 4$ Hz.

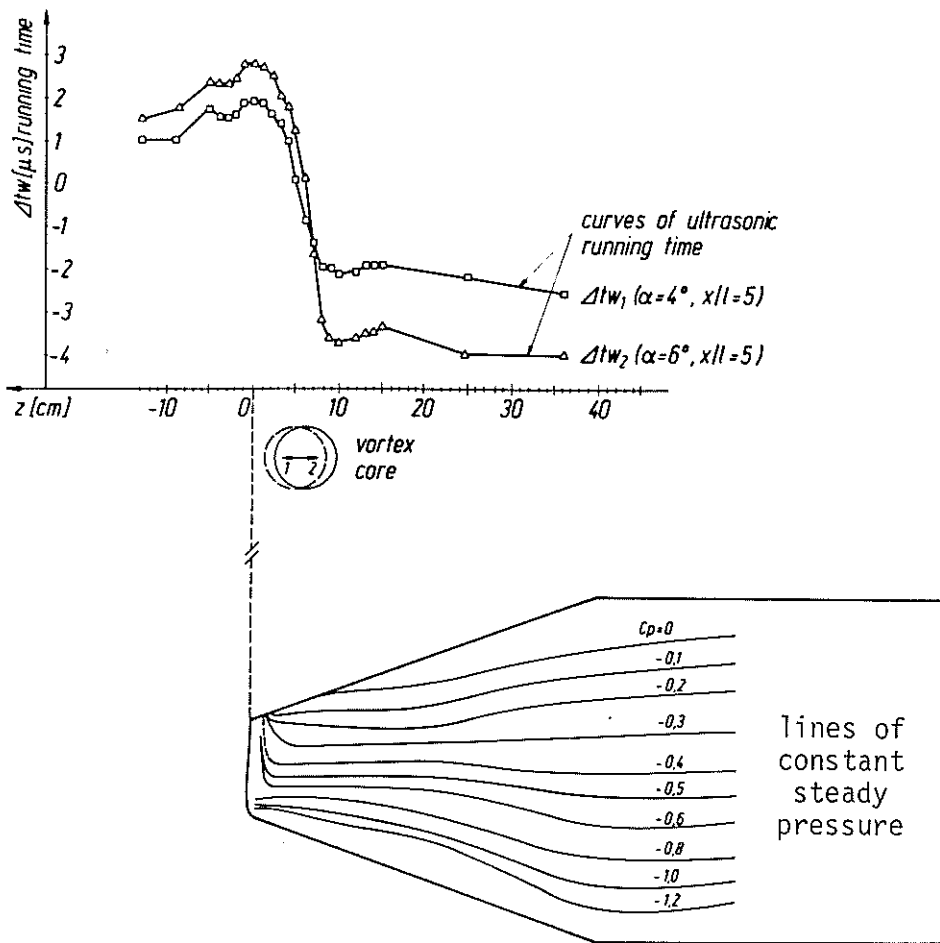


Figure 17: Graphs with equal scale in spanwise coordinate.

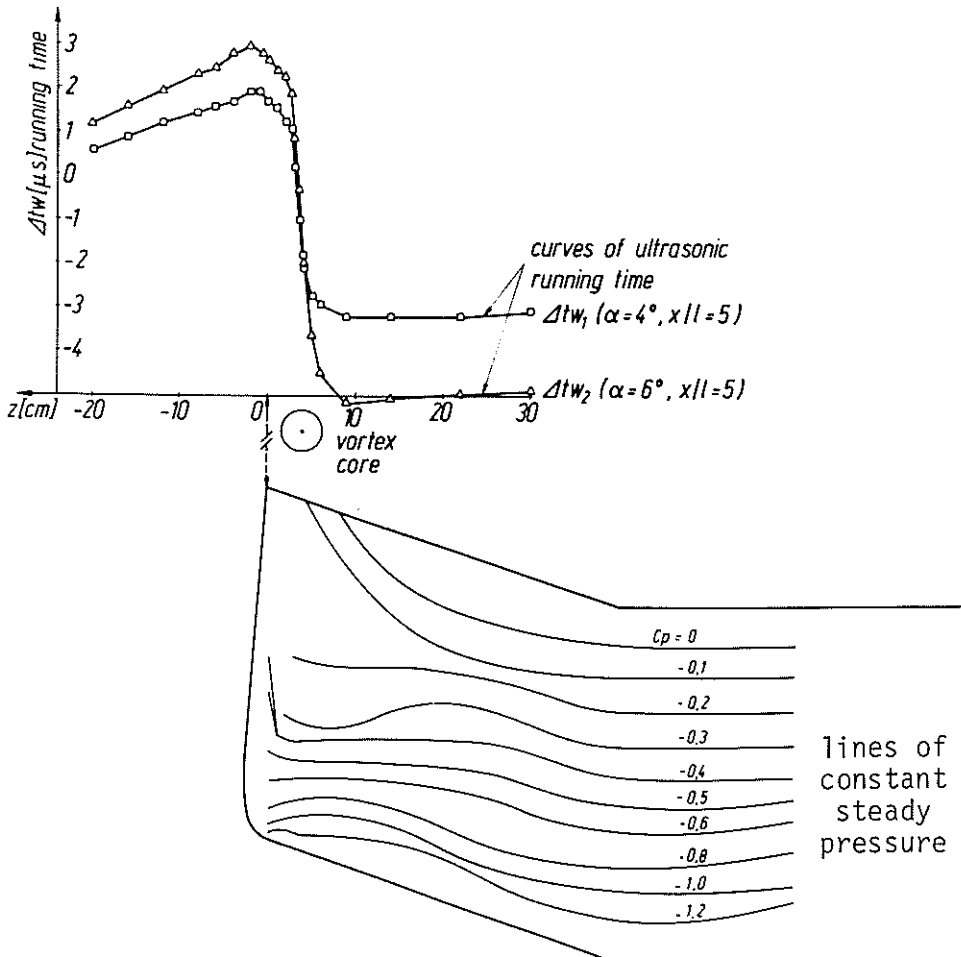


Figure 18: Graphs with equal scale in spanwise coordinate.

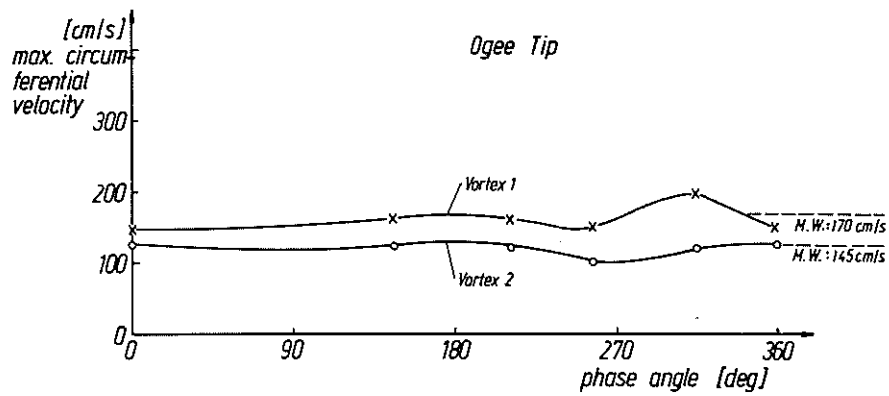


Figure 19: Variation of maximum circumferential velocity of the tip vortices versus phase angle of model pitch oscillation, $V = 20 \text{ m/s}$, $x/l = 2.75$, $\alpha_0 = 5^\circ$, $\Delta\alpha = \pm 1^\circ$, $f = 4 \text{ Hz}$.

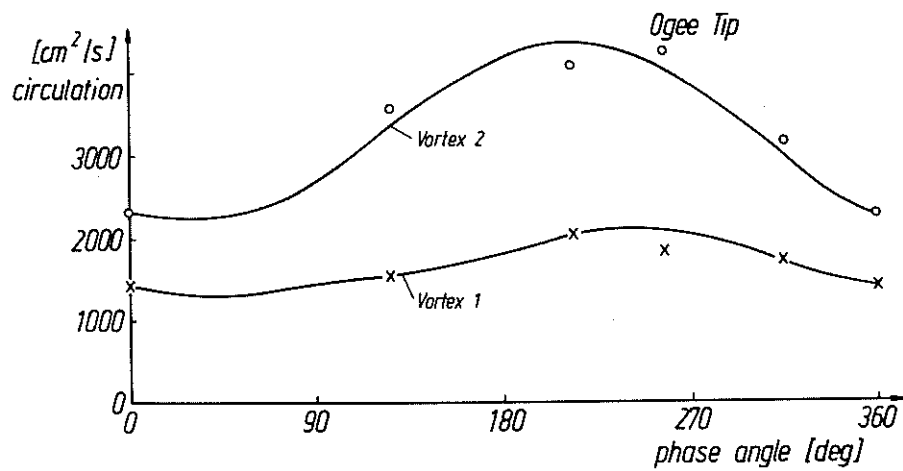


Figure 20: Variation of circulation of the tip vortices versus phase angle of model pitch oscillation, $V = 20 \text{ m/s}$, $x/l = 5$, $\alpha_0 = 5^\circ$, $\Delta\alpha = \pm 1^\circ$, $f = 4 \text{ Hz}$.

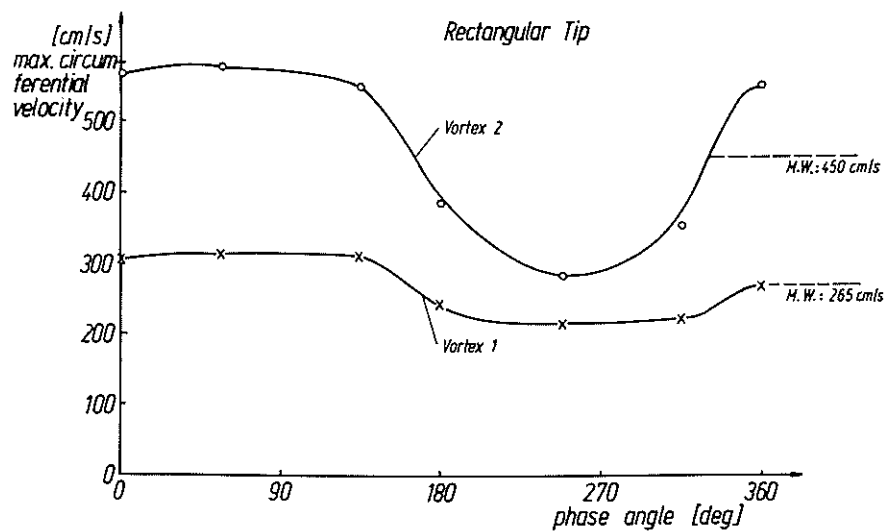


Figure 21: Variation of maximum circumferential velocity of the tip vortices versus phase angle of model pitch oscillation, $V = 20 \text{ m/s}$, $x/l = 2.75$, $\alpha_0 = 5^\circ$, $\Delta\alpha = \pm 1^\circ$, $f = 4 \text{ Hz}$.

In order to bring some systematic viewpoint into the somewhat confusing properties of the tip vortices, Figure 22 shows in table form some selected tip vortex characteristics of the four tip configurations. From the point of view (smallest velocity in the vortex) as indicated in the introduction, the Ogee tip appears to be the best configuration, followed by the trapezoidal tip.





| shape | number of vortex cores in the tip vortex structure | diameter of cores | maximum velocities in the vortices | shift of spanwise vortex position if incidence is altered: $\Delta\alpha = \pm 1^\circ$ |
|---|--|------------------------|------------------------------------|---|
| Rectangular Tip  | 2 | 1. 1.5 cm 2. 1.6 cm | 310 cm/s 590 cm/s | 0 |
| Ogee Tip  | 2 | 1. 2.0 cm 2. 5.6 cm | 160 cm/s 120 cm/s | ± 1.8 cm |
| Swept Tip  | 1 | 2 cm | 500 cm/s | 0 |
| Trapezoidal Tip  | 1 | 2.6 cm | 370 cm/s | ± 0.8 cm |

Figure 22: Table of tip characteristics, $V = 20$ m/s, mean incidence $\alpha_0 = 5^\circ$, ($\Delta\alpha = \pm 1^\circ$, $f = 4$ Hz), downstream position $x/l = 5$.

5. References

- [1] D.W. Schmidt, Acoustical Method for Fast Detection and Measurement of Vortices in Wind Tunnels, ICIASF'75 Record, 1975, pp.216-228.
- [2] K. Kienappel, Einfluß der Blattspitzengeometrie auf die instationäre Druckverteilung an einem Rotorblatt. Teil I: Rechteckblattspitze, DFVLR-IB 82-11, 1982.
- [3] J.B. Rorke, R.C. Moffitt, Wind Tunnel Simulation of Full-Scale Vortices, NASA CR-2180, 1973.
- [4] B. Maskew, Unsteady Potential Flow Analysis of Rotor Blade Tip Shapes, Interim Report, 1980.
- [5] W.J. McCroskey, J.J. Philippe, Unsteady Viscous Flow on Oscillating Airfoils, AIAA Journ. Vol.13, No.1, 1975, pp.71-79.
- [6] K. Kienappel, H. Stange, W. Wagner, Instationäre Druckverteilungsmessung an einem Rotationsellipsoid, DFVLR-FB 80-18, 1980.
- [7] R.H. Engler, W.J. Wagner, B. Weitemeier, Experimental Study of Tip Vortices behind an Oscillating Blade by the Ultra-Sonic Method, Proc. Collog. honoring H.G.Küssner on occ. of 80th birthday, Göttingen 1980, pp.119-129.
- [8] W. Wagner, Comparative Measurements of the Unsteady Pressures on Three Oscillating Wing-Tip Models, DFVLR-FB 84-07, 1984.
- [9] W. Send, Schwingende Tragflächen und ihr Nachlauf, DFVLR-Nachrichten, 1984, S.13-18.